HUMAN MUTATION 23:552–558 (2004)

RESEARCH ARTICLE

Identification of a New Complementation Group of the Peroxisome Biogenesis Disorders and *PEX14* as the Mutated Gene

Nobuyuki Shimozawa,[1]* Toshiro Tsukamoto,[2] Tomoko Nagase,[1] Yasuhiko Takemoto,[1] Naoki Koyama,[2] Yasuyuki Suzuki,[3] Masayuki Komori,[4] Takashi Osumi,[5] Gootjes Jeannette,[6] Ronald J.A. Wanders,[6] and Naomi Kondo[1]

[1]*Department of Pediatrics, Gifu University School of Medicine, Gifu, Japan;* [2]*Genomics Research Institute, Utsunomiya University, Utsunomiya, Japan;* [3]*Medical Education Development Center, Gifu University School of Medicine, Gifu, Japan;* [4]*Laboratory of Cellular and Molecular Biology, Department of Veterinary Science, Graduate School of Agriculture and Biological Sciences, Osaka Prefecture University, Osaka, Japan;* [5]*Department of Life Science, Himeji Institute of Technology, Hyogo, Japan;* [6]*Department of Clinical Chemistry and Pediatrics, Academic Medical Centre, University of Amsterdam, The Netherlands*

Communicated by Jean-Louis Mandel

Peroxisome biogenesis disorders (PBD) are lethal hereditary diseases caused by abnormalities in the biogenesis of peroxisomes. At present, 12 different complementation groups have been identified and to date, all genes responsible for each of these complementation groups have been identified. The peroxisomal membrane protein PEX14 is a key component of the peroxisomal import machinery and may be the initial docking site for the two import receptors PEX5 and PEX7. Although *PEX14* mutants have been identified in yeasts and CHO-cells, human *PEX14* deficiency has apparently not been documented. We now report the identification of a new complementation group of the peroxisome biogenesis disorders with *PEX14* as the defective gene. Indeed, human *PEX14* rescues the import of a PTS1-dependent as well as a PTS2-dependent protein into the peroxisomes in fibroblasts from a patient with Zellweger syndrome belonging to the new complementation group. This patient was homozygous for a nonsense mutation in a putative coiled-coil region of PEX14, c.553C>T (p.Q185X). Furthermore, we showed that the patient's fibroblasts lacked PEX14 as determined by immunocytochemical analysis. These findings indicate that there are 13 genotypes in PBD and that the role of PEX14 is also essential in humans. Hum Mutat 23:552–558, 2004 © 2004 Wiley-Liss, Inc.

KEY WORDS: complementation group; peroxisome biogenesis disorders; PBD; *PEX14*; protein import, Zellweger syndrome; ZS

DATABASES:
PEX14 – OMIM:601791, 601539 (PBD), 214100 (ZS); GenBank: AF045186.1; Ensembl Genome Browser: ENSG00000142655

INTRODUCTION

Peroxisomal disorders, an expanding group of genetic disorders in man, are generally divided into two groups with disorders of peroxisome biogenesis and single peroxisomal enzyme deficiencies. The peroxisome biogenesis disorders (PBD; MIM# 601539) include Zellweger syndrome (ZS; MIM# 214100), neonatal adrenoleukodystrophy (NALD; MIM# 202370), infantile Refsum disease (IRD; MIM# 266510), and rhizomelic chondrodysplasia punctata Type 1 (RCDP1; MIM# 215100). PBD are genetically heterogeneous and have so far been classified into 12 complementation groups (CGs). *PEX* genes encode peroxins, proteins involved in and necessary for peroxisome biogenesis, and the *PEX* genes responsible for 11 of the 12 complementation groups have been identified. These include: *PEX1* (PBD group 1 or E at Gifu), *PEX2* (group 10 or F at Gifu), *PEX3* (group 12 or G at Gifu), *PEX5* (group 2), *PEX6* (group 4 or C at Gifu), *PEX7* (RCDP; group 11 or R at Gifu), *PEX10* (group 7 or B at Gifu), *PEX12* (group 3), *PEX13* (group 13 or H at Gifu), *PEX16* (group 9 or D at Gifu), and *PEX19* (group 14 or J at Gifu) [Gould et al., 2001; Shimozawa et al., 1998]. Very recently, Matsumoto et al. [2003a,b] identified *PEX26* as the gene mutated in group 8 (A at Gifu), which means that so far all responsible genes of these 12 CGs have been identified.

Received 28 July 2003; accepted revised manuscript 6 January 2004.

*Correspondence to: Dr. Nobuyuki Shimozawa, Division of Genomics Research, Life Science Research Center, Gifu University, 1–1 Yanagido, Gifu 501–1193, Japan. E-mail: nshim@cc.gifu-u.ac.jp

Grant sponsor: Japan Society for the Promotion of Science; Grant number 13670791; Grant sponsor: Ministry of Health, Labour, and Welfare; Grant number: 14C-3.

DOI 10.1002/humu.20032
Published online in Wiley InterScience (www.interscience.wiley.com)

These peroxins can be divided into two major categories: factors required for peroxisome membrane biogenesis, including their import, and peroxisomal matrix protein import. In PBD, *PEX3*, *16*, and *19* are involved in the former, *PEX 1*, *2*, *5*, *6*, *7*, *10*, *12*, *13*, and *26* in the latter. Peroxisomal matrix proteins are synthesized on cytosolic ribosomes and are recognized by PTS receptors, PEX5 and PEX7, and then receptor-ligand complexes are thought to dock at the peroxisomal membrane. The *PEX14* gene (MIM# 601791) has been cloned in yeasts [Albertini et al., 1997; Komori et al., 1997] and codes for a peroxisomal membrane protein that binds to the PEX5 and PEX7. The PEX14 is thought to be the initial docking site for the receptors at the peroxisome membrane, and to form a docking complex with PEX13 [Girzalsky et al., 1999]. A human homolog of the yeast *PEX14* gene was cloned (GenBank accession number: AF045186.1) [Fransen et al., 1998; Will et al., 1999]; however, there is no evidence as to whether or not human *PEX14* is required for not only PTS import but also for multiple metabolic processes in humans. To date, more than 20 *PEX* genes have been identified in yeasts, but only 12 *PEX* genes involved in peroxisome biogenesis in humans have been discovered.

We report here that human *PEX14* gene restores matrix protein import in fibroblasts from a newly identified CG of PBD.

MATERIALS AND METHODS

Patient

The patient (K-01) was born after an uneventful pregnancy and showed the typical craniofacial dysmorphia including large open fontanelles, high forehead, flat occiput, low/broad nasal bridge, and micrognathia plus neurologic abnormalities, including hypotonia, suggestive of ZS. Plasma analysis revealed elevated very long chain fatty acids (VLCFA), di- and trihydroxycholestanoic acid and a normal phytanic acid level. Erythrocyte plasmalogens were undetectable. The patient died at 10 days of age. No autopsy was allowed, and no permission was given for a liver biopsy. A skin biopsy, however, was taken, allowing detailed studies to be performed in cultured fibroblasts.

Complementation and Microscopic Analysis

Complementation tests on human fibroblasts from various PBD patients were done by restoration of peroxisomes by means of immunocytochemical staining of catalase in fused cells [Yajima et al., 1992]. Peroxisomes in fibroblasts were visualized by indirect immunofluorescence light microscopy, as described previously [Shimozawa et al., 1992], using rabbit antibodies to human catalase, human 70 kDa PMP (PMP70) [Imanaka et al., 1996], rat peroxisomal acyl-CoA oxidase (AOX) [Suzuki et al., 1992], D-bifunctional protein (DBP) [Suzuki et al., 1997], peroxisomal 3-ketoacyl CoA thiolase (PT) [Suzuki et al., 1992], and PEX14 [Komori et al., unpublished data]. For observation we used a confocal laser-scanning microscope (LSM5 PASCAL, Carl Zeiss, www.zeiss.com).

Mutation Analysis of *HsPEX14* in Group K Patient

HsPEX14 cDNA was synthesized from fibroblast RNA by RT-PCR. The coding region of the cDNA (1-1134, nucleotide numbering uses the A of the ATG translation initiation start site as nucleotide +1; GenBank accession number: AF045186.1) was amplified by PCR, with primer sets 5′-GAAAGATGGCGTCCTCGGAG-3′ ([-5]-15) and 5′-TCAGAGAGACCGGCCTCCAT-3′ (461-442) to obtain a 466-bp product ([-5]-461), 5′-ATGGCAGGCATTGCATTTGG-3′ (346-365) and 5′-AAGTGGTAGGTGACCGTGGA-3′ (875-856) to obtain a 530-bp product (346-875), and 5′-GATCCCAGTCAAGTCACCGT-3′ (726-745) and 5′-ACACTAGATGCCATCCTCAG-3′ (1177-1158) to obtain a 452-bp product (726-1177), 40 cycles of 94°C for 1 min, 55°C for 1 min, and 72°C for 1 min. The amplified DNA fragments were directly sequenced using an automated DNA sequencer. As the c.553C>T (p.Q185X) mutation created the *Mae* I site at the 552 in the *HsPEX14* cDNA, the 530-bp PCR products (346-875) obtained from a control and K-01 cDNA were digested with *Mae* I. Genomic DNA fragments, containing p.Q185X in the *PEX14*, were obtained from cultured fibroblasts K-01 and the control by PCR, 40 cycles of 94°C for 1 min, 55°C for 1 min, and 72°C for 1 min, with primer sets 5′-AGCGCCGTGACTGCTTTCTC-3′ and 5′-CCTGTGCAGCAGAGACAGGT-3′ (Emsembl Genome Browser: ENSG00000142655). The amplified DNA fragment was directly sequenced.

Plasmids and Transfection into Fibroblasts From K-01 Patient

pGFPSKL has been described previously [Hashiguchi et al., 2002] and pPTS2-GFP, which encodes GFP, with N-terminal 32 amino acid residues of PT as peroxisome targeting signal 2. pECFPNLS was made by insertion of oligonucleotides (5′-CCCCCCAAGAAGAAGCGCAAGGTGCG-3′ and 5′-AGCTCCCCCCAAGAAGAAGCGCAAGGTGCGAATT-3′) encoding the nuclear localization signal of SV40 T antigen into the SacI/EcoRI sites of pECFP-C1 (Clontech, www.clontech.com). Full-length *HsPEX14* cDNA expression plasmid, named pUcD2-*PEX14*, was constructed into pUcD2SRalphaMCS [Tsukamoto et al., 1995] with the two partial human cDNA clones (I.M.A.G.E. clone ID143924 and 304848). p.Q185X mutation was introduced into pUcD2*PEX14* using two complementary oligonucleotides, 5′-CAGCAGCAGAAGATCTAGGAGCTTGCCCAC-3′ and 5′-GTGGGCAAGCTCCTAGATCTTCTGCTGCTG-3′. Mutation was confirmed by sequencing.

To clarify peroxisomal protein import in the K-01 patient, 3 μg of pGFPSKL or pPTS2-GFP were transfected into the K-01 fibroblasts (1×10^4 in a 35-mm dish) using modified calcium phosphate methods [Chen and Okayama, 1987]. To assess the complementation activity of *PEX14*, 2.1 μg of pUcD2*PEX14* (wild-type or p.Q185X) and 0.9 μg of one of three GFP constructs were used. Cells were fixed 48 hr after transfection, and intracellular localization of GFPSKL or PTS2-GFP was observed. Images were taken using QED software and an Olympus BX50 fluorescence microscope equipped with a color CCD camera (Cool SNAP, Photometrics, www.photomet.com). Cells transfected with pECFPNLS were further stained with anti-human catalase and Cy3-labelled anti-rabbit IgG antibody (Jackson Immunoresearch Laboratories, www.jacksonimmuno.com), and cells with punctate catalase staining among the transfected cells (nuclear ECFP positive cells) were assessed. A black-and-white CCD camera (1312M-FW-TE, DVC, Inc., www.dvcco.com) was used.

Other Methods

VLCFAs and plasmalogen were detected using a selected ion monitoring-electron impact method and 5×10^5 of fibroblasts, as described previously but with slight modification [Takemoto et al., 2003].

RESULTS

Studies in Fibroblasts From the Group K Patient

The VLCFAs ratio of C26:0/C22:0 was elevated in fibroblasts from the patient (K-01 fibroblasts) (0.336) compared to the control (0.041 ± 0.025). The absolute

values of plasmalogen (C16:0 DMA) showed decreased levels in K-01 fibroblasts (0.154) compared to the control (1.298 ± 0.534). Immunofluorescence studies revealed no punctate immunofluorescence with anti-catalase (Fig. 1B) and a few particle-bound immunofluorescences with anti-AOX, -DBP, and -PT antibody (Fig. 1F, H, and J) in the K-01 fibroblasts, in contrast to numerous particles in the control (Fig. 1A, E, G, and I). To assess import efficiency of newly synthesized protein with PTS into peroxisomes, transient transfection of the pGFPSKL and pPTS2-GFP was performed. A clear difference was observed; there was no PTS1 and PTS2 protein import in the K-01 fibroblasts (Fig. 1L and N), whereas almost all GFP was imported into peroxisomes in the control (Fig. 1K and M). These results indicate that K-01 fibroblasts affected both PTS1 and PTS2 protein import. Subsequently, complementation analysis was done and formation of peroxisomes in the majority of multinuclear cells was detected after fusion between fibroblasts from the patient and fibroblasts from the 11 groups, exclusive of CG 11 (R at Gifu), which manifested RCDP phenotype and affected only PTS2 protein import (data not shown). These results indicate the existence of a new complementation group, K (Table 1). In the study of peroxisomal ghost membrane protein, using an anti-PMP70 antibody, many PMP70-containing particles were seen in K-01 fibroblasts as in the control (Fig. 1C and D). Furthermore, after 7d incubation at 30°C, a definite punctate staining pattern was not detected in fibroblasts from K-01 (data not shown), suggesting that K-01 fibroblasts had no temperature sensitive (TS) phenotypes of the peroxisome assembly process [Imamura et al., 1998].

Expression of HsPEX14: Restoration of PTS1 and PTS2 Protein Import in Fibroblasts From Patient of Group K

Three proteins, catalase, GFP-SKL, and PTS2-GFP, were chosen to judge complementation by *PEX14*,

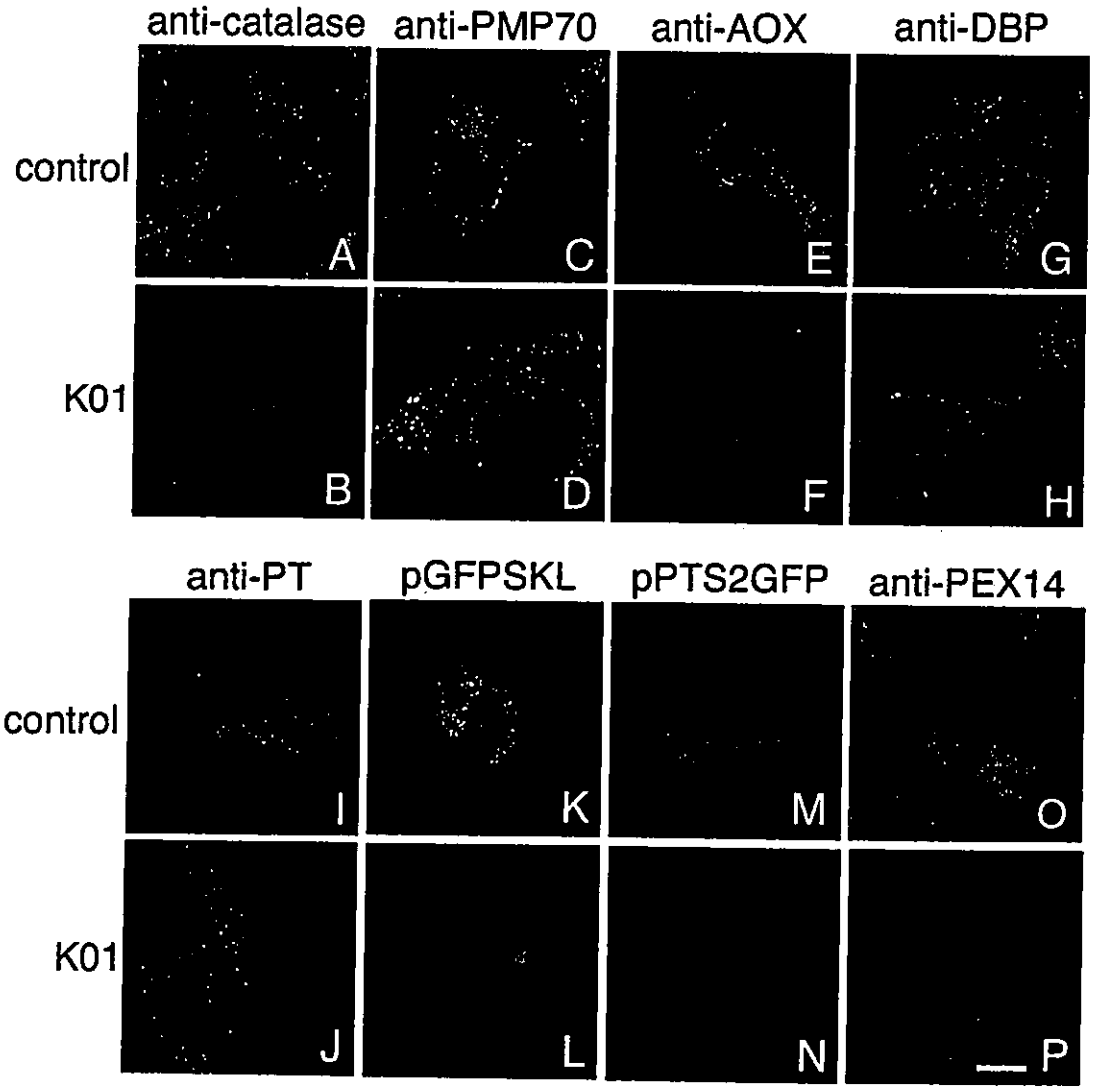

FIGURE 1. Fibroblasts from K-01 patient. **A, C, E, G, I,** and **O:** Fibroblasts from control. **B, D, F, H, J,** and **P:** K-01 fibroblasts. Cells were stained using antibodies to human catalase (A and B), human PMP70 (C and D), AOX (E and F), DBP (G and H), PT (I and J), and PEX14 (O and P). Control fibroblasts transfected with pGFPSKL (**K**) and pPTS2-GFP (**M**). K-01 fibroblasts transfected with pGFPSKL (**L**) and pPTS2-GFP (**N**). Bar = 20 μm.

because they never showed punctate localization in the K-01 cells (Fig. 1B, L, and N). In the K-01 fibroblasts co-transfected with pUcD2*PEX14* and pECFPNLS, particle-bound immunofluorescent staining with anti-human catalase was seen (Fig. 2A) among transfected cells (nuclear CFP positive cells, data not shown). Percent of import restoring cells was low at 26% (Table 2) and there was still strong cytoplasmic catalase staining. In contrast, import of GFP-SKL as well as PTS2-GFP was efficiently restored. Numerous punctate fluorescence without cytoplasmic fluorescence was seen in the K-01 fibroblasts co-transfected with pUcD2*PEX14* and two different plasmids, pGFPSKL (Fig. 2C) and pPTS2-GFP (Fig. 2E) (Table 2), yet there was no particle in cells singly transfected in the K-01 fibroblasts with pGFPSKL (Fig. 1L) and pPTS2-GFP (Fig. 1N). These findings mean that *HsPEX14* rescues the PTS1 and PTS2 protein import in K-01 fibroblasts.

Mutation Analysis of HsPEX14 in Group K Patient

To determine the dysfunction of *PEX14* in the patient of K-01, the coding region of the complete cDNA for *HsPEX14* was RT-PCR amplified. Direct sequencing of cDNA from the K-01 indicated a single point mutation (C>T) at position 553 (c.553C>T) in a codon 185 Gln, resulting in creation of termination codon TAG (designated "p.Q185X") (Fig. 3A). As this c.553C>T (p.Q185X) mutation formed the *Mae* I site in *HsPEX14* cDNA, the 530-bp PCR products (875-856) obtained from a control and K-01 cDNA were digested with *Mae* I. The PCR products obtained from the control were not sensitive to *Mae* I, whereas K-01 was completely digested with *Mae* I (Fig. 3B). These results suggest that the K-01

TABLE 1. Complementation Groups of Peroxisomal Biogenesis Disorders*

	Gifu	Phenotypes	Ghost peroxisomes	Gene
1	E	ZS, NALD, IRD	+	*PEX1*
2		ZS, NALD, IRD	+	*PEX5*
3		ZS, NALD, IRD	+	*PEX12*
4	C	ZS, NALD	+	*PEX6*
7	B	ZS, NALD	+	*PEX10*
8	A	ZS, NALD, IRD	+	*PEX26*
9	D	ZS	-	*PEX16*
10	F	ZS, IRD	+	*PEX2*
11	R	RCDP	+	*PEX7*
12	G	ZS	-	*PEX3*
13	H	ZS, NALD	+	*PEX13*
14	J	ZS	-	*PEX19*
	K	ZS	+	*PEX14*

*Gifu, complementation grouping of Gifu University School of Medicine; ZS, Zellweger syndrome; NALD, neonatal adrenoleukodystrophy; IRD, infantile Refsum disease; RCDP, rhizomelic chondrodysplasia punctata.

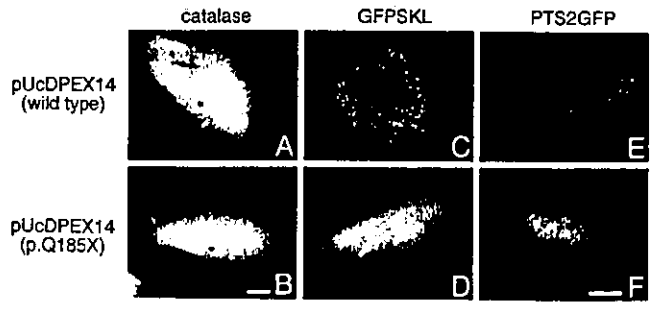

FIGURE 2. Complementation of fibroblasts from K-01 patient. PUcD2*PEX14* was cotransfected into the K-01 fibroblasts with pECFPNLS (**A**), pGFPSKL (**C**), and pPTS2-GFP (**E**). PUcD2-*PEX14*/p.Q185X was cotransfected into the K-01 fibroblasts with pECFPNLS (**B**), pGFPSKL (**D**), and pPTS2-GFP (**F**). Cells were stained using an antibody to human catalase and a Cy3-labelled anti-rabbit IgG antibody (A and B). Bar = 20 μm.

TABLE 2. Properties of Restoration to Protein Import in Wild and Mutant *PEX14*-transfected K-01 Fibroblasts

	Anti-catalase	pGFPSKL	pPTS2-GFP
pUcD2*PEX14* (wild type)	7/27*	19/20	136/180
pUcD2*PEX14*/p.Q185X	0/38	0/22	0/40
Bluescript	0/32	0/32	0/40

*Import-restoring cells/transfectant cells.

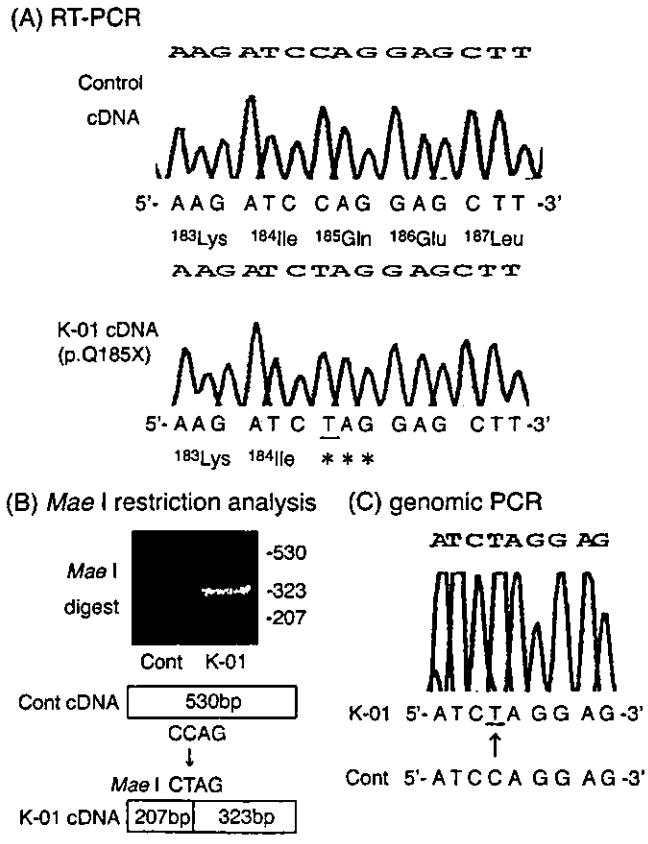

FIGURE 3. Mutation analysis of *PEX14* from complementation group K patient. **A:** Partial nucleotide sequence and deduced amino acid sequence of *PEX14* cDNA isolated from a normal control (upper) and the K-01 patient (lower) are shown. A point mutation of nucleotide C to Tat position 553 (c.553C>T) in a codon 185 Gln, resulting in creation of termination codon TAG (p.Q185X). **B:** *Mae* I restriction analysis for detection of the c.553C>T (p.Q185X) mutation in *PEX14* cDNA. Each PCR-amplified fragment (530 bp) of *PEX14*cDNA, derived from a control and K-01, was electrophoresed on 2% agarose gel after digestion with *Mae* I. **C:** Partial nucleotide sequence of *PEX14* genomic DNA isolated from the K-01 patient is shown. Only a single type of nucleotide sequence giving rise to the c.553C>T (p.Q185X) mutation was identified.

patient was homozygous for the c.553C>T mutation at the cDNA level. To determine the zygosity of a c.553C>T mutant allele, genomic PCR was done to amplify the 150-bp product, containing c.553C>T in the *PEX14* from the K-01 fibroblasts. Only a single type of nucleotide sequence giving rise to the c.553C>T mutation was identified in the PCR product (Fig. 3C). The result was interpreted to mean that the K-01 patient was homozygous for the c.553C>T (p.Q185X) mutation ([c.553C>T]+[c.553C>T]). When pUcD2*PEX14*/p.Q185X was transfected back with pECFPNLS into the K-01 fibroblasts, no particle stained by anti-catalase antibody was seen (Fig. 2B, Table 2). Furthermore, when pUcD2*PEX14*/p.Q185X was cotransfected with pGFPSKL and pPTS2-GFP into the K-01 fibroblasts, no punctata was seen in these transfectants (Fig. 2D, F), whereas numerous punctata were seen in the co-transfectants of pUcD2*PEX14* (Fig. 2C, E) (Table 2), which implies that the p.Q185X mutation may affect function for peroxisomal protein imports of the PEX14.

Immunonegative for PEX14 in the Fibroblasts From the Patient

When fibroblasts from the K-01 patient were evaluated by immunocytochemistry with antibody to PEX14, no punctate immunofluorescence was seen (Fig. 1P), in contrast to numerous particles in the control (Fig. 1O).

DISCUSSION

The 26 *PEX* genes-encoding proteins required for the biogenesis of peroxisomes, including the formation of the peroxisomal membrane and import of proteins into the peroxisomal matrix, have been identified. In humans, 12 genetic groups have been identified among the peroxisome biogenesis disorders, and all of the human *PEX* genes defective in each of these complementation groups have been clarified [Matsumoto et al., 2003b].

In our present study, we identified a new complementation group number 13 with *PEX14* as the defective gene. Indeed, *HsPEX14* rescues the import of the PTS1- and PTS2-dependent protein to peroxisomes in fibroblasts from the index patient belonging to complementation group K (K-01 fibroblasts). Furthermore, patient K-01 was homozygous for a nonsense mutation of PEX14, p.Q185X, and the data on transfection of this mutated *HsPEX14* into the K-01 fibroblasts confirmed that impaired *PEX14* is the genetic cause of the newly identified CG-K. We confirmed the absence of immunocytochemical staining for the PEX14 in fibroblasts from the patient. Thereby, *PEX14* is the 13th gene responsible for the PBD.

PEX14 gene was cloned in *S. cerevisiae* (*ScPEX14*) [Albertini et al., 1997] and *H. polymorpha* (*HpPEX14*) [Komori et al., 1997]. ScPEX14 and HpPEX14, peripheral peroxisomal membrane proteins exposed to the cytoplasm, are required for both PTS1 and PTS2 protein import. ScPEX14 may mediate the membrane docking event of PTS2 dependent protein import, and also interacts with PEX5 and several other peroxins including PEX13, the putative docking protein for PTS1 dependent protein import. Studies on the interaction in ScPEX14 suggested that C-terminal SH3 domain of PEX13 might bind a PXXP-peptide of ScPEX14 [Pires et al., 2003].

In mammals, rat *PEX14* (*RnPEX14*) was isolated by functional complementation of a peroxisome-deficient CHO mutant, which was deficient in both PTS1- and PTS2-mediated import [Shimizu et al., 1999]. Our immunofluorescence studies revealed that in the PTS1-dependent proteins, no catalase-containing particle and few particles stained by DBP and AOX were seen in fibroblasts from patient K-01, which means few AOX and DBP may be able to be imported into peroxisomes, whereas catalase could not be imported at all. A similar finding was observed also in the case of PTS2-dependent protein, PT; that is, few particles stained by PT were seen in the patient's fibroblasts. These findings have been already noted in the fibroblasts from *PEX5*-deficient patients and demonstrate that dysfunction of import into peroxisomes in each matrix protein was different not only between PTS1- and PTS2-dependent proteins but also among the PTS1-dependent proteins. We also suggested KANL (PTS1 sequences of the catalase) was a poorer variant of PTS1 and was likely to be more susceptible to effects of mutation of the PEX [Shimozawa et al., 1999]. The defect in PTS1 and PTS2 import was restored by transfection with the wild-type *HsPEX14* into K-01 fibroblasts but was not restored when the mutant *HsPEX14* was transfected (Fig. 2, Table 2). Additionally, biochemical analysis revealed that the VLCFAs ratio of C26:0/C22:0 was elevated in the K-01 fibroblasts and that plasmalogen content was reduced. Each biochemical abnormality depended on the function of the PTS1- and PTS2-dependent proteins, respectively. Taken together, the *PEX14*-deficient human PBD patient also affects both PTS1 and PTS2-mediated import, which means that PEX14 is required for both PTS1- and PTS2-dependent protein import even in humans.

In membrane topology of the mammalian PEX14, both the C-terminus and N-terminus is exposed to the cytosol and this peroxin interacts with PEX5, PEX13, PEX19, and itself [Fransen et al., 1998; Will et al., 1999; Shimizu et al., 1999; Otera et al., 2000; Oliveira et al., 2002]. The deduced 377-amino acid protein, HsPEX14, contains a nonmembrane-spanning hydrophobic region (amino acid residues [aa] 109–127) and a putative coiled-coil region (aa 138–200), and this peroxin binds to both the PEX5 and weekly with the SH3 domain of PEX13 [Fransen et al., 1998]. Shimizu et al. [1999] also reported that RnPEX14 apparently contained at least one hydrophobic segment (a putative membrane-spanning segment; aa 112–136 of both RnPEX14 and HsPEX14) and a predicted coiled-coil region (aa 159–197 of both RnPEX14 and HsPEX14), and they suggested that RnPEX14 might bind in a homometric manner, as based on binding assay data. Furthermore, Oliveira et al. [2002] reported that homopolymerization of HsPEX14 involved a domain comprising aa 147–278 of this peroxin, containing a predicted coiled-coil motif,

which means this portion may be essential for the PEX14 function. The p.Q185X mutation in the K-01 patient avoided this portion, and our expression experiments demonstrated that this mutated *PEX14* failed in recovery of the protein import (Fig. 2, Table 2). Similarly, the C-terminally truncated HpPEX14 (ΔC124) showed a defect in import of PTS1 protein, alcohol oxidase [Bellu et al., 2001]. These data indicate that the K-01 patient affects PEX14 caused by truncation at the coiled-coil region of this peroxin. Taken together, we have identified a new complementation group of the peroxisome biogenesis disorders (group K) and have identified the defective gene that codes for a truncated PEX14. Our findings indicate that all of the responsible genes in 13 genotypes of PBD have been identified (Table 1), and that the genetic basis of the peroxisome biogenesis disorders is more heterogeneous than previously considered. We wish to stress the importance of doing detailed studies in each individual PBD patient.

ACKNOWLEDGMENTS

We thank R. Horibe for technical assistance; M. Ohara for helpful comments; T. Hashimoto and N. Usuda for anti-AOX, -DBP, and -PT antibodies; and T. Imanaka for anti-human PMP70 antibody.

REFERENCES

Albertini M, Rehling P, Erdmann R, Girzalsky W, Kiel JA, Veenhuis M, Kunau WH. 1997. Pex14p, a peroxisomal membrane protein binding both receptors of the two PTS-dependent import pathways. Cell 89:83–92.

Bellu AR, Komori M, van der Klei IJ, Kiel JAW, Veenhuis M. 2001. Peroxisome biogenesis and selective degradation converge at Pex14p. J Biol Chem 276:44570–44574.

Chen C, Okayama H. 1987. High-efficiency transformation of mammalian cells by plasmid DNA. Mol Cell Biol 7: 2745–2752.

Fransen M, Terlecky SR, Subramani S. 1998. Identification of a human PTS1 receptor docking protein directly required for peroxisomal protein import. Proc Natl Acad Sci USA 95: 8087–8092.

Girzalsky W, Rehling P, Stein K, Kipper J, Blank L, Kunau WH, Erdmann R. 1999. Involvement of Pex13p in Pex14p localization and peroxisomal targeting signal 2-dependent protein import into peroxisomes. J Cell Biol 144:1151–1162.

Gould SJ, Raymond GV, Valle D. 2001. The peroxisome biogenesis disorders. In: Scriver CR, Beaudet AL, Sly WS, Valle D, editors. The metabolic and molecular basis of inherited disease. 8th ed. New York: McGraw-Hill. p 3181–3217.

Hashiguchi N, Kojidani T, Imanaka T, Haraguchi T, Hiraoka Y, Baumgart E, Yokota S, Tsukamoto T, Osumi T. 2002. Peroxisomes are formed from complex membrane structures in PEX6-deficient CHO cells upon genetic complementation. Mol Biol Cell 13:711–722.

Imamura A, Tsukamoto T, Shimozawa N, Suzuki Y, Zhang Z, Imanaka T, Fujiki Y, Orii T, Kondo N, Osumi T. 1998. Temperature-sensitive phenotypes of peroxisome-assembly processes represent the milder forms of human peroxisome-biogenesis disorders. Am J Hum Genet 62:1539–1543.

Imanaka T, Shiina Y, Takano T, Hashimoto T, Osumi T. 1996. Insertion of the 70-kDa peroxisomal membrane protein into peroxisomal membranes in vivo and in vitro. J Biol Chem 271:3706–3713.

Komori M, Rasmussen SW, Kiel JA, Baerends RJ, Cregg JM, van der Klei IJ, Veenhuis M. 1997. The Hansenula polymorpha PEX14 gene encodes a novel peroxisomal membrane protein essential for peroxisome biogenesis. EMBO J 16:44–53.

Matsumoto N, Tamura S, Fujiki Y. 2003a. The pathogenic peroxin Pex26p recruits the Pex1p-Pex6p AAA ATPase complexes to peroxisomes. Nat Cell Biol 5:454–460.

Matsumoto N, Tamura S, Furuki S, Miyata N, Moser A, Shimozawa N, Moser HW, Suzuki Y, Kondo N, Fujiki Y. 2003b. Mutations in novel peroxin gene PEX26 that cause peroxisome-biogenesis disorders of complementation group 8 provide a genotype-phenotype correlation. Am J Hum Genet 73:233–246.

Oliveira ME, Reguenga C, Gouveia AM, Guimaraes CP, Schliebs W, Kunau WH, Silva MT, Sa-Miranda C, Azevedo JE. 2002. Mammalian Pex14p: membrane topology and characterization of the Pex14p-Pex14p interaction. Biochim Biophys Acta 1567: 13–22.

Otera H, Harano T, Honsho M, Ghaedi K, Mukai S, Tanaka A, Kawai A, Shimizu N, Fujiki Y. 2000. The mammalian peroxin Pex5pL, the longer isoform of the mobile peroxisome targeting signal (PTS) type 1 transporter, translocates the Pex7p. PTS2 protein complex into peroxisomes via its initial docking site, Pex14p. J Biol Chem 275:21703–21714.

Pires JR, Hong X, Brockmann C, Volkmer-Engert R, Schneider-Mergener J, Oschkinat H, Erdmann R. 2003. The ScPex13p SH3 domain exposes two distinct binding sites for Pex5p and Pex14p. J Mol Biol 326:1427–1435.

Shimizu N, Itoh R, Hirono Y, Otera H, Ghaedi K, Tateishi K, Tamura S, Okumoto K, Harano T, Mukai S, Fujiki Y. 1999. The peroxin Pex14p. cDNA cloning by functional complementation on a Chinese hamster ovary cell mutant, characterization, and functional analysis. J Biol Chem 274:12593–12604.

Shimozawa N, Tsukamoto T, Suzuki Y, Orii T, Shirayoshi Y, Mori T, Fujiki Y. 1992. A human gene responsible for Zellweger syndrome that affects peroxisome assembly. Science 255:1132–1134.

Shimozawa N, Suzuki Y, Zhang Z, Imamura A, Kondo N, Kinoshita N, Fujiki Y, Tsukamoto T, Osumi T, Imanaka T, Orii T, Beemer F, Mooijer P, Dekker C, Wanders RJ. 1998. Genetic basis of peroxisome assembly mutants of humans, CHO cells and yeast: identification of a new complementation group of peroxisome biogenesis disorders, absent from peroxisomal membrane ghosts. Am J Hum Genet 63:1898–1903.

Shimozawa N, Zhang Z, Suzuki Y, Imamura A, Tsukamoto T, Osumi T, Fujiki Y, Orii T, Barth PG, Wanders RJ, Kondo N. 1999. Functional heterogeneity of C-terminal peroxisome targeting signal 1 in PEX5-defective patients. Biochem Biophys Res Commun 262:504–508.

Suzuki Y, Shimozawa N, Yajima S, Orii T, Yokota S, Tashiro Y, Osumi T, Hashimoto T. 1992. Different intracellular localization of peroxisomal proteins in fibroblasts from patients with aberrant peroxisome assembly. Cell Struct Funct 17:1–8.

Suzuki Y, Jiang LL, Souri M, Miyazawa S, Fukuda S, Zhang Z, Une M, Shimozawa N, Kondo N, Orii T, Hashimoto T. 1997. D-3-hydroxyacyl-CoA dehydratase/D-3-hydroxyacyl-CoA dehydrogenase bifunctional protein deficiency: a newly identified peroxisomal disorder. Am J Hum Genet 61:1153–1162.

Takemoto Y, Suzuki Y, Horibe R, Shimozawa N, Wanders RJA, Kondo N. 2003. Gas chromatography/mass spectrometry analysis of very long chain fatty acids, docosahexaenoic acid, phytanic acid and plasmalogen for the screening of peroxisomal disorders. Brain Dev 25:481–487.

Tsukamoto T, Miura S, Nakai T, Yokota S, Shimozawa N, Suzuki Y, Orii T, Fujiki Y, Sakai F, Bogaki A, Yasumo H, Osumi T. 1995. Peroxisome assembly factor-2, a putative ATPase cloned by functional complementation on a peroxisome-deficient mammalian cell mutant. Nat Genet 11:395–401.

Will GK, Soukupova M, Hong X, Erdmann KS, Kiel JA, Dodt G, Kunau WH, Erdmann R. 1999. Identification and characterization of the human orthologue of yeast Pex14p. Mol Cell Biol 19:2265–2277.

Yajima S, Suzuki Y, Shimozawa N, Yamaguchi S, Orii T, Fujiki Y, Osumi T, Hashimoto T, Moser HW. 1992. Complementation study of peroxisome-deficient disorders by immunofluorescence staining and characterization of fused cells. Hum Genet 88: 491–499.

Available online at www.sciencedirect.com
SCIENCE DIRECT®
Biochemical and Biophysical Research Communications 317 (2004) 181–186
BBRC
www.elsevier.com/locate/ybbrc

Generation of highly stable IL-18 based on a ligand–receptor complex structure

Yutaka Yamamoto, Zenichiro Kato,* Eiji Matsukuma, Ailian Li, Kentaro Omoya, Kazuyuki Hashimoto, Hidenori Ohnishi, and Naomi Kondo

Department of Pediatrics, Gifu University School of Medicine, Tsukasa 40, Gifu 500-8705, Japan

Received 30 January 2004

Abstract

Human interleukin-18 (hIL-18), initially cloned as an IFN-γ-inducing factor, has a key role in many inflammatory diseases. We have previously developed a high production system for correctly folded active hIL-18 protein, leading to the revelation of the 3D-structure and the receptor binding mode. These findings can strongly indicate the experimental and medical applications of IL-18; however, the recombinant protein is prone to be inactivated forming multimers. Recently, therapeutic approaches using recombinant IL-18 have shown the effectiveness for treatment of cancer; indicating the necessity of a more stable protein for therapy with intertrial reliability. Here we have generated a highly stable hIL-18 with replacement of cysteine by serine based on the tertiary structure and the binding mechanism, retaining the biological activity. Similar rational designs can be applied to develop new therapeutic molecules of other cytokines.

Keywords: IL-18; Mutant; Cysteine; Stability; 3D-structure

Human interleukin-18 (hIL-18), initially cloned as an IFN-γ-inducing factor secreted by macrophages or Kupffer cells, strongly augments the production of IFN-γ both in natural killer cells and T cells; having a key role in many inflammatory diseases including allergy and autoimmune diseases [1–3]. We previously developed a high production system of correctly folded active hIL-18 protein, and it enabled us to determine both the 3D-structure and the molecular mechanism of the receptor binding mode [4,5]. This production method and the molecular mechanisms can strongly assist in the experimental and medical applications of IL-18; however, one of the most common problems of recombinant protein usage for experiments and medicine is the inactivation of the protein, usually forming aggregates [6]. Recently, therapeutic approaches using recombinant IL-18 have been examined for treatment of cancer including a clinical trial in humans; indicating the necessity for a more stable form that will allow therapy to be undertaken with intertrial reliability [7–9].

Here, we describe the generation of highly stable hIL-18 based on the tertiary structure and the binding mechanism. The mutant protein with replacement of cysteine by serine showed marked antioxidative stability without formation of the oligomers, and there was no reduction in biological activity.

Materials and methods

Vector construction and protein expression. Construction of the expression vector, expression, and purification of wild type hIL-18 protein were carried out as described previously [4]. Briefly, the coding region for mature hIL-18 (157 residues) with FactorXa cleavage site just before the hIL-18 sequence was amplified by PCR and the amplified product was cloned into the pGEX-4T-1 vector (Pharmacia). BL21 (DE3) (Novagen) was transformed by the vector, and protein expression was performed as follows: the colony with the highest expression level was cultivated overnight in 200 ml of the LB medium with 100 μg/ml ampicillin. The culture was transferred into 2 L of the LB medium with 100 μg/ml ampicillin and then incubated at 37 °C until the OD600 = 0.45; it was then cooled to 25 °C. IPTG (final concentration 1 mM) was added to the medium when OD600 = 0.5. The culture was further incubated at 25 °C for 5 h.

A bacterial cell pellet was resuspended in lysis buffer (50 mM Tris–HCl, pH 8.0, 400 mM KCl, 10 mM of 2-mercaptoethanol (2ME), and

* Corresponding author. Fax: +81-58-265-9011.
E-mail address: zen-k@cc.gifu-u.ac.jp (Z. Kato).

0006-291X/$ - see front matter © 2004 Elsevier Inc. All rights reserved.
doi:10.1016/j.bbrc.2004.03.024

1 mM EDTA) with 1 mM PefaBloc (Roche), lysed by sonication, and centrifuged. The clear lysate was applied onto a GST affinity column (Pharmacia) and the column was then washed. The captured fusion protein was eluted with elution buffer (50 mM Tris–HCl, pH 8.0, and 10 mM glutathione). The protein-containing fractions were concentrated and cleaved by bovine factor-Xa (Funakoshi) at a ratio of 1% (w/w) at 4 °C. The mature hIL-18 protein was isolated using Sephacryl S-100 26/60 (Pharmacia). The fractions were then stored at 4 °C until further experiments.

Oligomerization assay of the wild protein. Oligomerization assay of the protein using wild type protein was carried out in a sealed siliconized Eppendorf tube. The protein solution (400 ng/μl) in phosphate-buffered saline (NaCl 137 mM, Na_2HPO_4 8.10 mM, KCl 2.68 mM, and KH_2PO_4 1.47 mM, pH 7.0) was agitated at 150 rpm at 37 °C for 12 h in the incubator. The sample solution was mixed with 5* concentrated SDS–sample buffer (final concentration 2% (w/v) SDS, 10% (v/v) glycerol, 0.002% (w/v) bromophenol blue, 62.5 mM Tris–HCl, pH 6.8, and with/without 5% (v/v) of 2ME) and boiled for 5 min. The samples were electrophoresed on SDS–PAGE (10–20% gradient gel) and visualized by Coomassie blue staining.

Structural analyses of hIL-18 and the receptor complex. Multiple sequence alignments of the IL-18 s were performed by ClustalW with BLOSUM matrix [10]. The structure of the hIL-18 (PDB code: 1J0S) was determined by us using nuclear magnetic resonance (NMR); and here we used the modeled structure of the hIL-18:hIL18R α complex for structural analyses [5]. Structural rendering was performed on RasMol software [11].

Production and analyses of the mutant proteins. Site-directed mutagenesis of the hIL-18 gene was performed using GeneEditor in vitro Site-Directed Mutagenesis System (Promega) according to the manufacturer's instructions. Four different primers were designed for mutations to serine at C38, C68, C76, and C127, respectively. The primer sequences were: C38S: 5′-GACTGATTCTGACTCTAGAGATAATG CACC-3′, C68S: 5′-CTATCTCTGTGAAGT CTGAGAAAATTTCA ACTC-3′, C76S: 5′-GAAAATTTCAACTCTCTCCTCTGA GAACA AAA TTATTTCC-3′, (C68S/C78S for IL-18-AS: 5′-GTAACTAT CTCTGTGAAGTCTGAGAAAATTTCAACTCTCTCCTCTGAG AACAAAATTATTTCC-3′), and C127S: 5′-GATACTTTCTAG CTTCTGAAAAAGAGAGAG-3′ All the plasmid sequences harboring respective mutations were confirmed bidirectionally. Expression, purification, and the oligomerization assays were performed the same as those for wild type protein.

Biological activity assay. A biological activity assay based on IFN-γ induction was carried out as previously described [12]. Briefly, human myelomonocytic KG-1 cells were grown in the culture medium consisting of RPMI 1640 supplemented with 10% heat-inactivated fetal calf serum, L-glutamine (2 mmol/L), penicillin (100 U/mL) and streptomycin (100 μg/mL). KG-1 cells (3.0×10^5 cells) were cultured in the presence of 0.1–50.0 ng/mL of recombinant hIL-18 for 24 h in a volume of 0.2 ml at 37 °C in a humidified atmosphere containing 5% CO_2. The culture supernatant was centrifuged to remove cells and stored at −80 °C until assay was performed. IFN-γ concentration was measured by fluorometric microvolume assay technology using FMAT 8100HTS system (Applied Biosystems).

Results

Oligomerization assay of wild type IL-18

On SDS–PAGE, wild type protein showed a marked oligomerization pattern after aeration by agitation (Fig. 1). However, the oligomerization pattern completely disappeared in the presence of 2ME; indicating that it was mainly due to the intermolecular disulfide bonds among the cysteine residues of hIL-18.

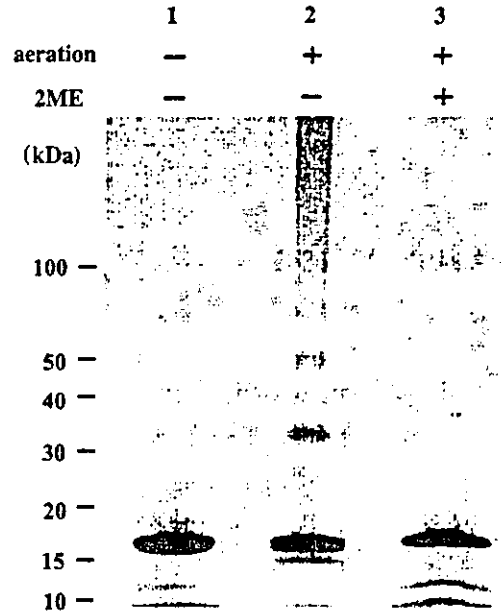

Fig. 1. Oligomerization assay of the wild type IL-18. Electrophoresis was carried on SDS–PAGE (10–20% gradient gel). (1) Before aeration without 2ME, (2) after aeration without 2ME, and (3) after aeration with 2ME. Four micrograms of each protein was loaded. The wild type protein shows a marked oligomerization pattern after aeration, but the pattern disappeared with 2ME.

Structural analyses of hIL-18 and the molecular mechanisms of receptor binding

Alignment of the amino acid sequences of the IL-18 proteins showed marked similarities among the different species. C76 and C127 are conserved among all the species, while C38 and C68 were replaced by the other residues in several species (Fig. 2). Conservation among different species usually indicates the importance of the conserved residues for the structure or activity; but conservation itself cannot show the positions of the residues in the 3D-structure associated with intra- or inter-molecular disulfide bonds.

The 3D-structure of hIL-18 determined by NMR clearly showed an absence of intramolecular disulfide bonds, and cysteine residues existing on the surface of the structure suggested a possible role for intermolecular disulfide bonds in the oligomerization (Fig. 3A). The atomic interactions among the cysteine residues and the other residues of hIL-18, and also the positions of the cysteine residues on the complex structure with hIL-18R α suggested that the replacement of the four cysteine residues by other types of amino acids, especially the conservative residue, serine, does not collapse the 3D-structure of hIL-18; retaining the capacity to bind to the receptor (Figs. 3A and B). According to structural analyses, five mutant proteins were designed (Table 1).

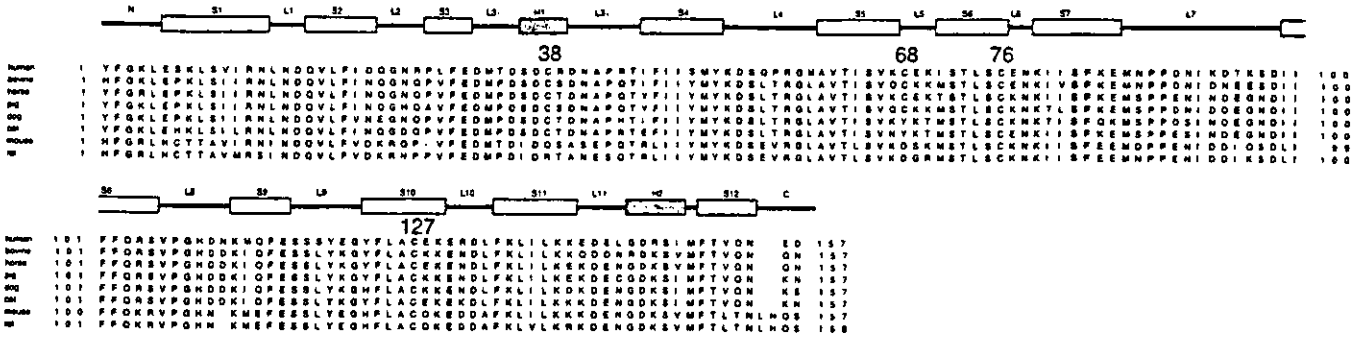

Fig. 2. Alignment of the amino acid sequences of IL-18 proteins. Completely conserved residues among the eight species are boxed in gray. The cysteine residues are boxed in yellow. The numbers of the cysteine residues are indicated as a human sequence. The secondary structure for human IL-18 previously determined by us is indicated over the sequences as the yellow (S; β-strand) and the blue (H; helix) boxes. The intermediate loop regions are indicated as L. C76 and C127 are conserved among all the species, while C38 and C68 were replaced by other residues in several species.

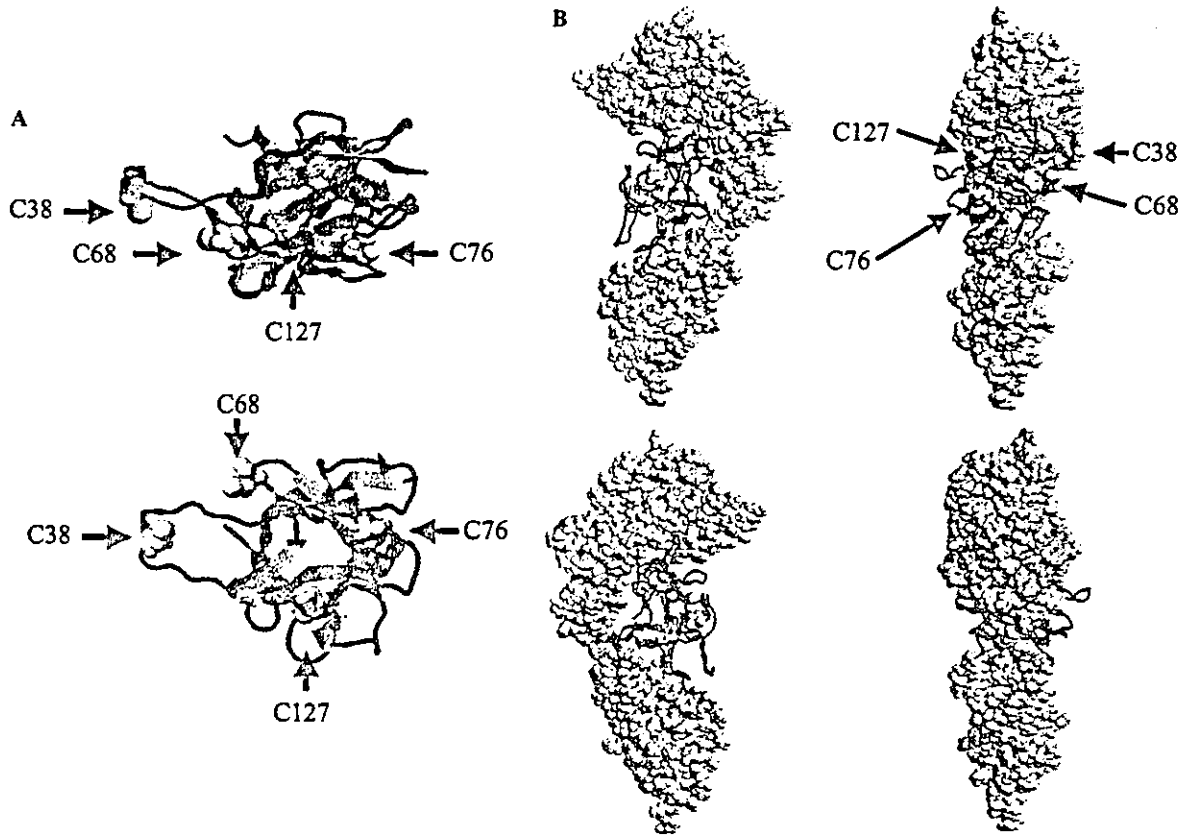

Fig. 3. Structure of the human IL-18 protein and the complex structure of human IL-18 and human IL-18 receptor α. (A) Structure of the human IL-18. The overall structure is shown as a ribbon model, and the four cysteine residues are shown as spacefill representation in yellow. The top figure and the bottom figure are tilted at 90° to each other. The four cysteine residues do not form any sulfide bonds and exist on the surface of the structure. (B) The complex structure of human IL-18 and human IL-18 receptor α. The overall structure of hIL-18 is shown as a ribbon model in cyan, and the four cysteine residues are shown as spacefill representations in yellow. hIL-18R α is shown as spacefill representation in white. The four cysteine residues of hIL-18 do not have any direct interaction with hIL-18R α; suggesting little influence on the binding.

Oligomerization assay of the IL-18 mutants

On SDS-PAGE, the mutants harboring one cysteine residue on the surface showed dimerization after the aeration procedure, but with different degrees (Figs. 4A and B). The findings indicate that all the cysteine residues of hIL-18 associated with the oligomerization phenomenon but to different extents. On the other hand, the IL-18-AS protein did not show any oligomerization pattern even after the aeration procedure (Fig. 5); indicating that the IL-18-AS protein can exist as a monomer in oxidative conditions.

Table 1
Amino acid composition of wild and mutant proteins

Position	38	68	76	127
Wild	Cys	Cys	Cys	Cys
C38	Cys	Ser	Ser	Ser
C68	Ser	Cys	Ser	Ser
C76	Ser	Ser	Cys	Ser
C127	Ser	Ser	Ser	Cys
AS	Ser	Ser	Ser	Ser

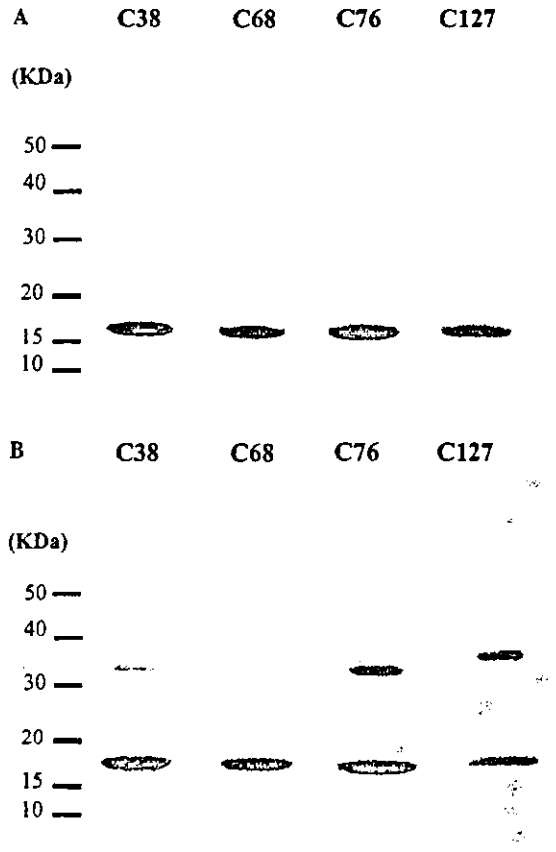

Fig. 4. Dimerization assay of the IL-18 mutants harboring one cysteine residue on the surface. Electrophoresis was carried out on SDS–PAGE (10–20% gradient gel). (A) Before aeration without 2ME, (B) and after aeration without 2ME. Four micrograms of each protein was loaded. All the mutants showed dimerization after aeration, indicating that all the cysteine residues of IL-18 associated with the oligomerization phenomenon.

Biological activity of wild and mutant protein, IL-18-AS

The biological activities of the wild type and IL-18-AS before aeration were compared. IFN-γ induction by different concentrations of the two IL-18 proteins showed no significant differences before oxidation (Fig. 6). The biological activities after aeration showed a marked reduction in the wild type protein; resulting in about five to ten times lower IFN-γ induction than that before oxidation between 1 and 10 ng/ml. However, IL-18-AS did not show any significant reduction even after extensive aeration (Fig. 6). These findings indicate

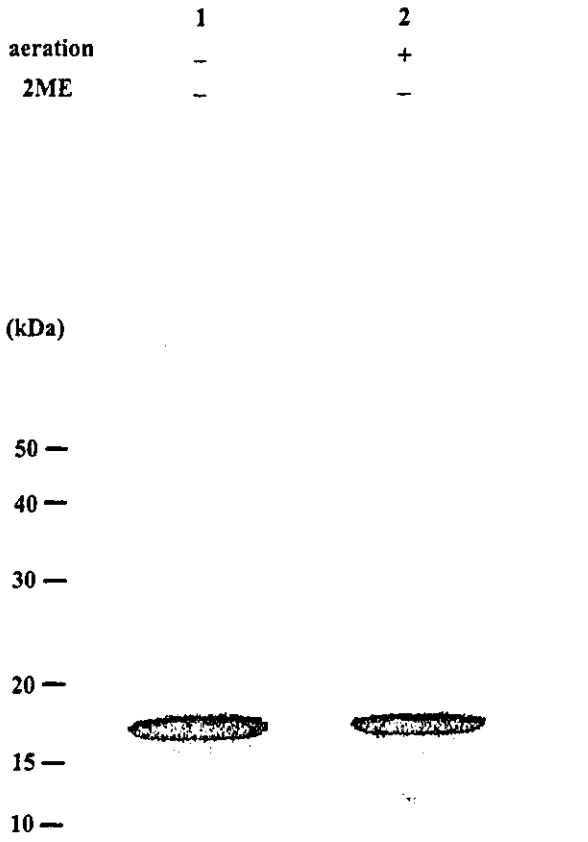

Fig. 5. Oligomerization assay of IL-18-AS. Electrophoresis was carried on SDS–PAGE (10–20% gradient gel). (1) Before aeration without 2ME, (2) after aeration without 2ME. Four micrograms of each protein was loaded. The IL-18-AS protein did not show any oligomerization pattern.

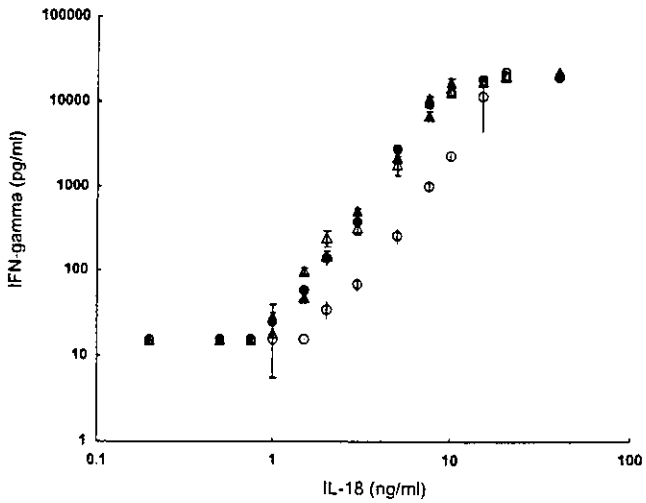

Fig. 6. IFN-γ induction (pg/ml) by the wild type and the IL-18-AS before and after oxidation. Mean values of triplicate IFN-γ induction assays are shown with standard deviation. Solid circle, hIL-18-wild before oxidation; open circle, hIL-18-wild after oxidation; solid triangle, hIL-18-AS before oxidation; and open triangle, hIL-18-AS after oxidation. IL-18-AS showed the same activity as that of the wild type even after oxidation, while wild type protein showed significant reduction in the activity after oxidation.

that the newly generated mutant, IL-18-AS, is highly stable against oxidative conditions; retaining the equivalent biological activity.

Discussion

Our method for the purification of hIL-18 shows that recombinant hIL-18 exist almost as a monomer in solution [4]. However, oligomerization and inactivation of IL-18 have been reported [13–15] and another of our studies also indicated that a small fraction of the purified protein existed as dimer or trimer even in an intensively reduced condition; suggesting that the IL-18 produced should be partially inactive [Kato et al. unpublished data]. However, the precise mechanisms of the inactivation have not yet been clarified.

Kikkawa et al. [14] speculated that one of the mechanisms of the inactivation should be misfolding; by the loss of the specific covalent intramolecular required for potent IFN-γ inducing function of IL-18, but the 3D-structure determined by us revealed that there are no intramolecular disulfide bonds in hIL-18 (Fig. 3). Further, the side chains of all the cysteine residues exist on the surface of the protein making it possible to be accessible by each other. From these observations, we can speculate that the oligomerization of IL-18 can be done using these free sulfatides on the molecular surface, and that the activity should be lost.

We have demonstrated here that wild type IL-18 forms extensive oligomers in oxidative conditions, and that the IFN-γ inducing activity was significantly reduced. The oligomerization mechanism is mediated by the intermolecular disulfide bonds among the four cysteine residues in IL-18 polypeptide, namely C38, C68, C76, and C127. To obtain an antioxidative stable hIL-18, we conservatively mutated all the cysteine residues to serine; and as the 3D-structure analyses predicted (Fig. 3), the resulting mutant protein, IL-18-AS, showed high stability retaining biological activity even after oxidation (Fig. 6).

In human fibroblast growth factor (hFGF), replacement of two of the four cysteine residues by serine (C70S and C88S) could improve instability; retaining the biological activities, but replaced the other two cysteine residues (C26S and C93S) resulting in a marked reduction in activity [16,17]. Biochemical analyses suggested that two cysteine residues (C26 and C93) form an intramolecular disulfide bond [17]. However, the structural determination of hFGF has revealed that C26 and C93 have no intramolecular sulfide bond with their side chains buried inside the molecule; indicating that the atomic interactions among the other residues will be important for the activity, while the side chains of C70 and C88 are exposed to the solvent without any disulfide bonds [18]. Moreover, the recent structure determination of the complex involving hFGF:FGF receptors has also revealed that C26 and C93 exist adjacent to the interface between ligand and receptor, while C70 and C88 are completely free from the interface of the receptor, similar to those observed in hIL-18 and the receptor [5,18].

Using a protein as a therapeutic agent requires not only production of a sufficient quantity of homogeneous protein, but also a stable formulation suitable for storage and delivery. The IL-18-AS protein that we have developed here showed significant stability against oxidation; retaining the same activity with wild type protein. Although recombinant hIL-18 has been examined in the treatment of cancer [7–9], the structure-based design of the mutants should be emphasized and the stable form of cytokine can be the first step for development of a more potent cytokine with additional site-specific modifications including glycosylation or pegylation [19–22].

Acknowledgments

We thank Prof. M. Shirakawa, Prof. K. Nishikawa, Dr. M. Mishima, Dr. T. Furuya, Dr. T. Yoneda, and Dr. T. Hara for their advice. Part of this work was supported by Uehara Memorial Foundation and by The Naito Foundation.

References

[1] H. Okamura, H. Tsutsui, T. Komatsu, M. Yutsudo, A. Hakura, T. Tanimoto, K. Torigoe, T. Okura, Y. Nukada, K. Hattori, K. Akita, M. Namba, F. Tanabe, K. Konishi, S. Fukuda, M. Kurimoto, Cloning of a new cytokine that induces IFN-γ production by T cells, Nature 378 (1995) 88–91.

[2] S. Ushio, M. Namba, T. Okura, K. Hattori, Y. Nukada, K. Akita, F. Tanabe, K. Konishi, M. Micallef, M. Fujii, K. Torigoe, T. Tanimoto, S. Fukuda, M. Ikeda, H. Okamura, M. Kurimoto, Cloning of the cDNA for human IFN-γ-inducing factor, expression in *Escherichia coli*, and studies on the biologic actives of the protein, J. Immunol. 156 (1996) 4274–4279.

[3] K. Nakanishi, T. Yoshimoto, H. Tsutsui, H. Okamura, Interleukin-18 is a unique cytokine that stimulates both Th1 and Th2 responses depending on its cytokine milieu, Cytokine Growth Factor Rev. 12 (2001) 53–72.

[4] A. Li, Z. Kato, H. Ohnishi, K. Hashimoto, E. Matsukuma, K. Omoya, Y. Yamamoto, N. Kondo, Optimized gene synthesis and high expression of human interleukin-18, Protein Expres. Purif. 32 (2003) 110–118.

[5] Z. Kato, J. Jee, H. Shikano, M. Mishima, I. Ohki, H. Ohnishi, A. Li, K. Hashimoto, E. Matsukuma, K. Omoya, Y. Yamamoto, T. Yoneda, T. Hara, N. Kondo, M. Shirakawa, The structure and binding mode of interleukin-18, Nat. Struct. Biol. 10 (2003) 966–971.

[6] T. Arakawa, S.J. Prestrelski, W.C. Kenney, J.F. Carpenter, Factors affecting short-term and long-term stabilities of proteins, Adv. Drug Deliv. Rev. 10 (1993) 1–28.

[7] K. Yamanaka, I. Hara, H. Nagai, H. Miyake, K. Gohji, M.J. Micallef, M. Kurimoto, S. Arakawa, S. Kamidono, Synergistic antitumor effects of interleukin-12 gene transfer and systemic

administration of interleukin-18 in a mouse bladder cancer model, Cancer Immunol. Immunother. 48 (1999) 297–302.
[8] H. Nagai, I. Hara, T. Horikawa, M. Fujii, M. Kurimoto, S. Kamidono, M. Ichihashi, Antitumor effects on mouse melanoma elicited by local secretion of interleukin-12 and their enhancement by treatment with interleukin-18, Cancer Invest. 18 (2000) 206–213.
[9] D.J. Herzyk, P.J. Bugelski, T.K. Hart, P.J. Wier, Preclinical safety of recombinant human interleukin-18, Toxicol. Pathol. 31 (2003) 554–561.
[10] P.A. Rastogi, MacVector. Integrated sequence analysis for the Macintosh, Methods Mol. Biol. 132 (2000) 47–69.
[11] R.A. Sayle, E.J. Milner-White, RASMOL: biomolecular graphics for all, Trends Biochem. Sci. 20 (1995) 374.
[12] K. Konishi, F. Tanabe, M. Taniguchi, H. Yamauchi, T. Tanimoto, M. Ikeda, K. Orita, M. Kurimoto, A simple and sensitive bioassay for the detection of human interleukin-18/interferon-gamma-inducing factor using human myelomonocytic KG-1 cells, J. Immunol. Methods 209 (1997) 187–191.
[13] T. Seya, M. Matsumoto, I. Shiratori, Y. Fukumori, K. Toyoshima, Protein polymorphism of human IL-18 identified by monoclonal antibodies, Int. J. Mol. Med. 8 (2001) 585–590.
[14] S. Kikkawa, M. Matsumoto, K. Shida, Y. Fukumori, K. Toyoshima, T. Seya, Human macrophages produce dimeric forms of IL-18 which can be detected with monoclonal antibodies specific for inactive IL-18, Biochem. Biophys. Res. Commun. 281 (2001) 461–467.
[15] S. Kikkawa, K. Shida, H. Okamura, N.A. Begum, M. Matsumoto, S. Tsuji, M. Nomura, Y. Suzuki, K. Toyoshima, T. Seya, A comparative analysis of the antigenic, structural, and functional properties of three different preparations of recombinant human interleukin-18, J. Interf. Cytok. Res. 20 (2000) 179–185.
[16] M. Seno, R. Sasada, M. Iwane, K. Sudo, T. Kurokawa, K. Ito, K. Igarashi, Stabilizing basic fibroblast growth factor using protein engineering, Biochem. Biophys. Res. Commun. 151 (1988) 701–708.
[17] G.M. Fox, S.G. Schiffer, M.F. Rohde, L.B. Tsai, A.R. Bank, T. Arakawa, Production, biological activity, and structure of recombinant basic fibroblast growth factor and an analog with cysteine replaced by serine, J. Biol. Chem. 263 (1988) 18452–18458.
[18] J. Schlessinger, A.N. Plotnikov, O.A. Ibrahimi, A.V. Eliseenkova, B.K. Yeh, A. Yayon, R.J. Linhardt, M. Mohammadi, Crystal structure of a ternary FGF–FGFR–heparin complex reveals a dual role for heparin in FGFR binding and dimerization, Mol. Cell 6 (2000) 743–750.
[19] T. Sareneva, J. Pirhonen, K. Cantell, I. Julkunen, N-glycosylation of human interferon-gamma: glycans at Asn-25 are critical for protease resistance, Biochem. J. 308 (1995) 9–14.
[20] S. Ohno, T. Yokogawa, I. Fujii, H. Asahara, H. Inokuchi, K. Nishikawa, Co-expression of yeast amber suppressor tRNATyr and tyrosyl-tRNA synthetase in *Escherichia coli*: possibility to expand the genetic code, J. Biochem. 124 (1998) 1065–1068.
[21] D. Kiga, K. Sakamoto, K. Kodama, T. Kigawa, T. Matsuda, T. Yabuki, M. Shirouzu, Y. Harada, H. Nakayama, K. Takio, Y. Hasegawa, Y. Endo, I. Hirao, S. Yokoyama, An engineered *Escherichia coli* tyrosyl-tRNA synthetase for site-specific incorporation of an unnatural amino acid into proteins in eukaryotic translation and its application in a wheat germ cell-free system, Proc. Natl. Acad. Sci. USA 99 (2002) 9715–9720.
[22] Y.S. Wang, S. Youngster, M. Grace, J. Bausch, R. Bordens, D.F. Wyss, Structural and biological characterization of pegylated recombinant interferon alpha-2b and its therapeutic implications, Adv. Drug Deliv. Rev. 54 (2002) 547–570.

Clinical features of Bloom syndrome and function of the causative gene (BLM helicase)

Hideo Kaneko† and Naomi Kondo

Bloom syndrome is a rare autosomal recessive genetic disorder characterized by growth deficiency, unusual facies, sun-sensitive telangiectatic erythema, immunodeficiency and predisposition to cancer. The causative gene for Bloom syndrome is *BLM*, which encodes the BLM RecQ helicase homolog protein. The first part of this review describes a long-term follow-up study of two Bloom syndrome siblings. Subsequently, the focus is placed on the functional domains of BLM. Laboratory diagnosis of Bloom syndrome by detecting mutations in *BLM* is laborious and impractical, unless there are common mutations in a population. Immunoblot and immunohistochemical analyses for the detection of the BLM protein using a polyclonal BLM antibody, which is a useful approach for clinical diagnosis of Bloom syndrome, are described. In addition, a useful adjunct for the diagnosis of Bloom syndrome in terms of the BLM function is investigated since disease cells must have the defective BLM helicase function. This review also discusses the nuclear localization signal of BLM, the proteins that interact with BLM and tumors originating from Bloom syndrome.

Expert Rev. Mol. Diagn. 4(3), (2004)

CONTENTS

†Author for correspondence
Department of Pediatrics, Gifu University Graduate School of Medicine, 1-1 Yanagido, Gifu 501-1194, Japan
Tel.: +81 58 230 6384
Fax: +81 58 230 6387
hideo@cc.gifu-u.ac.jp

Keywords:
associate protein, BLM, Bloom syndrome, cancer predisposition, DNA instability, functional domain, mutation, nuclear localization, RecQ helicase, screening for Bloom syndrome

The RecQ DNA helicase family includes five helicases: BLM, WRN, RecQ1, RecQ4 and RecQ5. They are the causative genes for many types of cancer, such as Bloom syndrome (BS), Werner syndrome and Rothmund–Thomson syndrome (*BLM*, *WRN* and *RecQ4*, respectively). These genes appear to maintain genomic stability [1–6]. Helicases are molecular motors that convert double-stranded nucleic acids into single-stranded molecules. To catalyze the disruption of hydrogen bonds that hold duplexes together, helicases use energy released from the hydrolysis of nucleotide 5′-triphosphates, usually ATP, to move along a strand of nucleic acid and unwind the duplex. The discovery of *recQ* in *Escherichia coli* in a screen for thymine-deficient, death-resistant mutants marked the identification of the first member of a large class of RecQ-related DNA helicases [7]. Several lines of study suggest that RecQ can suppress illegitimate recombination, thus helping to maintain genomic stability by preventing the formation of duplexes between imperfectly homologous DNA sequences. Therefore, the impairment of the RecQ helicase results in genomic instability and the development of various types of cancer. This paper describes the clinical features of BS and the function of the BLM gene.

Bloom syndrome: a long-term study of BS patients

A brother and sister in BS Registry were identified as HiOk and AsOk, respectively (TABLE 1) [8]. Clinical features included recurrent and prolonged middle ear and upper respiratory tract infections from the age of 2 years. This occured several times per year until about the age of 14 years for HiOk and 12 for AsOk. The severity and frequency of infections were lower in AsOk than in HiOk and as the they grew older, the recurrence of such infections gradually decreased. When HiOk began responding to therapy after the age of 16 years, the frequency of his middle ear infections decreased to once or twice per year at approximately 18 years of age.

Serum concentrations of the three major classes of immunoglobulin (Ig), IgM, IgG and IgA, were low at age 11 years in HiOk and at 9

 ISSN 1473-7159

for AsOk, compared with age-matched control means. However, the magnitude of reduction for each class of Ig varied. In both patients, serum concentrations of IgM were markedly low but those of IgG and IgA only mildly decreased. Neither patient has ever been administered γ-globulin therapy during the past 14 years. The small decrease in serum concentrations of IgG and IgA increased significantly with age, whereas the IgM levels remained low. Neither patient had a significantly reduced percentage of circulating $CD3^+$, $CD4^+$, $CD8^+$ or $CD19^+$ cells when compared with controls [9]. As already described, these patients showed the typical phenotype of BS.

Lymphoma

B-cell lymphoma

A prominent characteristic of BS is the high predisposition to various types of cancer [10]. After 1 month of treatment with exogenous insulin, HiOk developed B-cell non-Hodgkin's lymphoma, which responded to radiation (30 Gy) in the nasopharyngeal portion. However, after 5 months of treatment with radiation the lymphoma relapsed, with widespread abdominal disease that resisted chemotherapy. He died 24 months after the onset of the lymphoma from hepatic metastases [11,12].

AsOk complained of severe abdominal pain at 25 years of age and was diagnosed as having acute abdomnal lymphoma. A colon fiberscope revealed neoplastic changes of the epithelium around the ileum end and surgical treatment was subsequently performed. The tumor was located on the oral side, 30 cm from Bauhin's valve, and obstructed the intestinal cavity. It was diagnosed as B-cell non-Hodgkin's lymphoma. The patient received a half dose of the acute lymphoblastic leukemia protocol, which is used by the children's cancer study group (9104 standard risk protocol in the Tokai Pediatrics Oncology Study Group). The patient was also administrated the following drugs:

- Vincristine, 0.75 mg/m^2 on days 1, 8, 15, 22, 29, 71, 85, 99, 113, 127, 134 and 141
- Dexamethasone, 6 mg/m^2 on days 1–7 and 127–133
- Prednisolone, 30 mg/m^2 on days 8–14 and 134–140
- Prednisolone, 15mg/m^2 on days 15–28
- L-asparaginase, 5000 u/m^2 on days 15, 18, 21, 24, 27, 30, 87, 101 and 115
- Methotrexate 6 mg/m^2, cytarabine 15 mg/m2 and hydrocortisone 10 mg/m2 intrathecally on days 22, 29, 36, 43, 72, 86, 100 and 114
- Daunorubicin 15 mg/m^2 on days 43, 50 and 57
- Cytarabine, 35 mg/m^2 on days 44–47, 51–54 and 58–61
- Mercaptopurine, 25 mg/m^2 on days 36–63
- Methotrexate, 1500 mg/m^2 on days 85, 99 and 113 with leucovorin rescue
- Cyclophosphamide, 300 mg/m^2 on days 87, 101 and 115; pirarubicine, 15 mg/m^2 on days 127, 134 and 141
- Enocitabine, 50 mg/m^2 on days 128–131, 135–138 and 142–145

Table 1. Clinical features of two siblings with Bloom syndrome.

Features	HiOk	AsOk
Weight at birth	2100 g	2250 g
Height	143.1 cm (21 years old)	144.5 cm (19 years old)
Skin change	Telangiectatic erythema Brownish pigmentation with interspersed hypopigmented area Cafe-au-lait spots Atopic dermatitis	Cafe-au-lait spots Hypopigmented area
Facies	Malar hypoplasia Mandibular hypoplasia	Malar hypoplasia Mandibular hypoplasia
Intelligence	Within the normal range	Within the normal range
Immune system	Decreased IgM and IgA Increased IgE B-cell dysfunction	Decreased IgM and IgA Increased IgE B-cell dysfunction
Chromosome	Breakage of chromosome Increased SCEs	Breakage of chromosome Increased SCEs
Other findings	High-pitched voice Mild hepatic dysfunction Diabetes mellitus Small testes	Allergic rhinitis Early menopause

Ig: Immunoglobulin; SCE: Sister-chromatid exchange.

The patient continues complete remission and is free of treatment complications 5 years after diagnosis. It should be noted that BS displays chromosomal instability when chemotherapy for malignancy is performed.

Phenotype of B-cell lymphoma originating from HiOk

Pathological findings showed diffuse, large-cell lymphoma. Surface markers showed typical B-cell lineage without the expression of Ig chains. Also, Bcl-2 expression was not detected. The Cμ chain and overexpression of c-myc and p53 genes were not observed. Translocation of c-myc and Epstein–Barr virus (EBV) integration were not detected by Southern blotting.

p53 mutation of B-cell lymphoma

p53 mutations are often observed in B-cell lymphoma. The hot spots of p53 mutations from exons 5–9 were investigated. No cases showed p53 mutations in the genomic DNA extracted from neutrophils and lymphoma tissues from the original site. However, a metastatic lymphoma originating from the cecum of HiOk, 5 months after radiation therapy, showed a reduced length of the p53 exon 7. DNA sequence analysis revealed a 9 bp deletion in exon 7 (TABLE 2) [11].

Replication error

The BLM gene encodes a RecQ helicase homolog and the RecQ helicase is reportedly involved in some aspect of DNA replication. Therefore, dinucleotide and trinucleotide repeat replications on the X chromosome have been investigated. Lymphoma DNA from both the original and metasatic sites showed a reduced length of repetitive DNA, as determined by polyacrylamide gel electrophoresis. One EBV cell derived from HiOk B-cells also showed a reduced length of repetitive DNA. DNA sequence analysis of lymphoma in a recurrent site revealed a 6 or 3 bp deletion in a region of microsatellite DNA, HUMARA, and a 12 or 14 bp deletion in another region, DXS1113 (TABLE 2).

B-cell lymphoma and an EBV-transformed cell line derived from AsOk's B-cells did not show any changes in the length of repetitive DNA. Microsatellite instability has been detected in a variety of sporadic human tumors. This suggests that a mismatch repair deficiency could strongly accelerate malignant transformation of rapidly expanding cell populations. The function of the RecQ helicase, a homolog of BLM, is unclear, although it seems most likely to be one of the factors contributing to postreplication recombinational repair. Although there is no direct evidence that BLM participates in the mismatch repair system, the presence of microsatellite instability in lymphoma cells seems to suggest the direct or indirect involvement of BLM in that system.

It is possible that loss of helicase activity generates abnormal DNA structures during replication, which indirectly affects the activity of other DNA-binding proteins or activate repair mechanisms.

Ig gene rearrangement in BS lymphocytes

Almost all patients with BS have abnormally low concentrations of one or more of the plasma Ig and fail to show delayed hypersensitivity. The mechanisms of immunodeficiency remain to be elucidated. The involvement of BLM in DNA repair also remains to be determined. Werner syndrome is characterized by premature aging its causative gene, *WRN*, is homologous to *BLM*. However, immunodeficiency is not a characteristic clinical feature of Werner syndrome. BLM is preferentially expressed in the thymus and testes while WRN is ubiquitously and strongly expressed in the testes [13,14]. The difference in the expression patterns of BLM and WRN might explain the clinical features of immunodeficiency in BS. BLM expression was detected in all of the examined hematopoietic cell lines, although in varying amounts. It was assumed that a strong or low expression of BLM would appear to correlate with a fast or slow cell growth rate in each cell line. BLM expression in myelomonocytes was detected.

Table 2. Mutations in B-cell lymphoma originating from Bloom syndrome.

	Lymphona original site (HiOk)	Lymphona recurrence site (HiOk)	EB line (HiOk)	Lymphona original site (AsOk)	Lymphona EB line (AsOk)
p53	WT	9 bp deletion in exon 7 CTCACCATC[§]	WT	WT	ND
Dinucleptide repeat (DXS1113)	Deletion of one CT repeat and five CA repeats	Deletion of one CT repeat and five or six CA repeats	Deletion of one or two CT repeat and five or seven CA repeats	Germline[§§]	Germline[§§]
Trinucleotide repeat (HUMARA)	Deletion of two GCA repeats	Deletion of one or two GCA repeats	Deletion of two GCA repeats	Germline[§§]	Germline[§§]

[§]Mutation causes deletion of 3 amino acids (position 252-254).
[§§]Germline type was judged by detecting identical bands to neutrophil DNA.
ND: Not done; WT: Wild type.

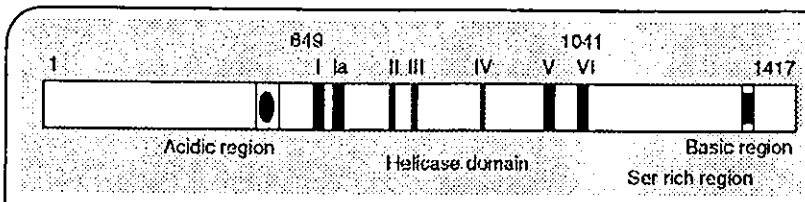

Figure 1. Features of BLM protein and functional motif. I to VI show the seven conserved helicase domains.

Although the function of myelomonocytes in BS has not been determined, this may explain why some BS patients with normal serum Ig concentrations are also susceptible to infection.

An increased frequency of abnormal T-cell rearrangement was observed in the peripheral blood lymphocytes (PBL) of patients with BS compared with control individuals. However, the frequency of abnormal rearrangement in the PBL of patients with BS is lower than the PBL in Ataxia-telangiectasia. Consistent with a previous report on peripheral B-cells from patients with BS, the sequences of the CDR3 region in the VDJ rearrangement were in-frame and insertion of the N region was also detected [15–17]. These results suggested that the DNA helicase function of BLM is not involved in VDJ recombination directly. Both T- and B-cells utilize the same machinery for VDJ recombination. BS cells have normal VDJ recombination in Ig, therefore it is not likely that the increased frequency of the abnormal T-cell receptor gene rearrangement in BS is caused by an abnormal catalytic function of the recombinase. The increased frequency of the abnormal T-cell rearrangement suggests that BLM is involved in the maintenance of DNA stability.

BLM gene & mutation

BLM was identified in 1995. It is 4437 bp long and encodes a 1417-amino acid peptide homologous to RecQ helicases, a subfamily of DExH box-containing DNA and RNA helicases (FIGURE 1) [18]. BLM is also highly homologous to the product of the yeast gene *SGS1* (slow-growth suppresser). It is assumed that the BLM protein plays an important role in the maintenance of genomic stability in somatic cells. In this syndrome, increased spontaneous sister-chromatid exchanges (SCEs) have been observed and it is believed to be the most malignancy-prone chromosomal disorder. The underlying lesion might be caused by a deficiency in DNA damage repair.

Ellis and German reported 14 unique mutations in 20 out of 25 people examined with BS. Three of the mutations were putative missence substitutions, six were nonsense mutations, two were frameshift mutations, two were exon-skipping mutations and one was a gross deletion detectable by Southern blot analysis (TABLE 3) [19]. The relatively high frequency of *BLM* mutations in the Ashkenazim has been reported as blmAsh, which is a 6 bp deletion/7 bp insertion at nucleotide 2281 in the open reading frame of *BLM*. This results in a frameshift and a stop codon at nucleotide 2292 [20,21]. Li and coworkers have reported that the blmAsh mutation is present in one out of 107 of this particular Ashkenazi Jewish population, a carrier frequency of 0.0093. However, a common mutation of *BLM* has not yet been reported in the other population. Furthermore, it is sometimes difficult to distinguish between BS and other DNA instability syndromes, such as the Fanconi or Rothmund–Thomson syndromes, based on clinical manifestations.

The mobility of the PCR-amplified *BLM* fragments from HiOk differed from that of healthy control DNA and was similar to that of AsOk DNA in acrylamide gel electrophoresis studies (FIGURE 2) [22]. PCR-amplified BLM fragments from their father and mother's DNA showed two bands, one with the same mobility as healthy control DNA and the other with the same mobility as HiOk and AsOk. A 3 bp deletion was detected in the *BLM* sequence from HiOk and AsOk DNA. This deletion caused the generation of a stop codon at amino acid 186. Both deleted and normal-sized BLM sequences were obtained from the father and mother's DNA.

Recent studies have identified a small increase in the risk of colorectal cancer developing in individuals who are heterozygous for the blmAsh allele [23]. Consistent with these studies, mice that are heterozygous for *BLM* mutations show enhanced tumorigenesis when infected with the murine leukemia virus or when crossed with mice that are heterozygous for the adenomatous polyposis of the colon (APC) tumor-suppressor gene [24]. This data indicates that *BLM* heterozygotes, other than those with the blmAsh allele, may be similarly cancer prone.

Functional domains of BLM

Nuclear localization signal in BLM

Based on previously published manuscripts whereby many BLM mutations truncate the protein upstream of the helicase domain, WRN mutations truncate the protein beyond the helicase domain. These WRN mutants probably retain DNA helicase activity. Lu and coworkers reported that site-directed mutations that eliminate the helicase activity of yeast SGS1 can still complement certain SGS1 mutants [25]. It is assumed that differenent disease symptoms caused by BLM and WRN mutations may be attributed to a loss of a function other than the helicase activity [26].

By searching for BLM amino acid sequences, putative bipartite nuclear localization signals (NLS) were found in the C-terminal domain (FIGURE 3) [27]. The fragments P-9, P-10 and P-11 were produced to correspond to the mutations previously reported in BS Registry designations 97, 112 and 93, respectively. The predicted peptides of the frameshift mutation observed in registry numbers 15, 42, 107 and NR2 were 739 amino acid residues and located between the fragments of P-7 and P-8. A green fluorescent protein (GFP) vector inserted with a full coding sequence of *BLM* was transfected into Hela

Table 3. BLM mutations identified in Bloom syndrome patients [19].

Mutations	Identification	Ancestry	Zygosity of the mutation	Nucleotide change	Protein change
Missense mutations	139(ViKre)	Mixed European	Heterozygous	A2089G	Q627R
	31 (CaDe)	Dutch	Heterozygous	A2089G	0627R
	40(DoRoe)	Mixed European	Heterozygous	G2776A	C901Y
	113(DaDem)	Italian	Homozygous	G3238C	C10558
Nonsense mutations	96(H:Ok)	Japanese	Homozygous	631delCAA	S186X
	112(NaSch)	Mixed European	Heterozygous	A888T	K272X
	98(RoMo)	Mixed European	Heterozygous	A1164	R364X
	81 (MaGrou)	French Canadian	Homozygous	C1858A	S595X
	11 (laTh)	Mixed European	Heterozygous	C2007T	Q645X
	61 (DoHop)	Mixed European	Homozygous	C2007T	Q645X
	NR1(ErBor)	Mixed European	Heterozygous	C2007T	Q645X
	NR8(KeSol)	Mixed European	Heterozygous	C2007T	Q645X
	51 (KeMc)	Mixed European	Homozygous	C2172T	0700X
Frame shift mutations	93 (YoYa)	Japanese	Homozygous	1610insA	514-1-X
	15(MaRo)	Ashkenazi Jewish	Homozygous	2281delATCTGAinsTA GATTC	735-4-X
	IQ 42(RAFR)	Ashkenazi Jewish	Homozygous	2281delATCTGAinsTA GATTC	735-4-X
	107(MyAsa)	Ashkenazi Jewish	Homozygous	2281defATCTGAinsTA GATTC	735-4-X
	NR2(CrSpe)	Ashkenazi Jewish	Homozygous	2281delATCTGAInsTA GATTC	735-4X
	(BrNa)	Ashkenazi Jewish	Heterozygous	2281de1ATCTGAinsTA GATTC	735-4-X
Exon-skipping mutations	IC 126(BrNa)	Ashkenazi/ Sepharadic	Heterozygous	Skip exon 2	
	112(NaSch)	Mixed European	Heterozygous	Skip exon 6	
	92(VaBia)	Italian	Homozygous	Skip exons 11 and 12	

cell lines, which express BLM abundantly, and GFP was found localized in the nucleus. A truncated form of BLM (by 1341 amino acids), containing only the proximal arm of basic amino acids, was not transported to the nucleus but instead remained in the cytoplasm. Another truncated form (by 1356 amino acids), containing two arms, was transported to the nucleus. The GFP vector inserted with DNA fragments with two arms of basic amino acids in the *C*-terminal, X–1, was also transported to the nucleus. The fragments with only the distal arm, X-2, were transported to the nucleus. These results suggest that the distal arm of the basic residues in the BLM protein is essential for nuclear localization. Truncated BLM proteins corresponding to previously reported BLM mutations were retained in the cytoplasm or both the cytoplasm and the nucleus. The distribution of both the cytoplasm and nucleus observed in the short BLM fragments, which were P-9 to P-11, might reflect the characteristics of GFP itself. In these cases, even if such short BLM fragments are transported to the nucleus, they could not have a function due to the defective helicase domain.

Full BLM and WRN proteins differ in length by only 15 residues and share a highly conserved helicase domain. Both the *N*- and *C*-terminal domains are unique to BLM and WRN, respectively, and these unique domains play a role in expressing disease symptoms. The nuclear localization signal of BLM was identified and, in addition, WRN also has the functional NLS in its *C*-terminus. These results were acceptable, considering that helicases catalyze the unwinding of double-stranded DNA to provide single-strand templates in the nucleus.

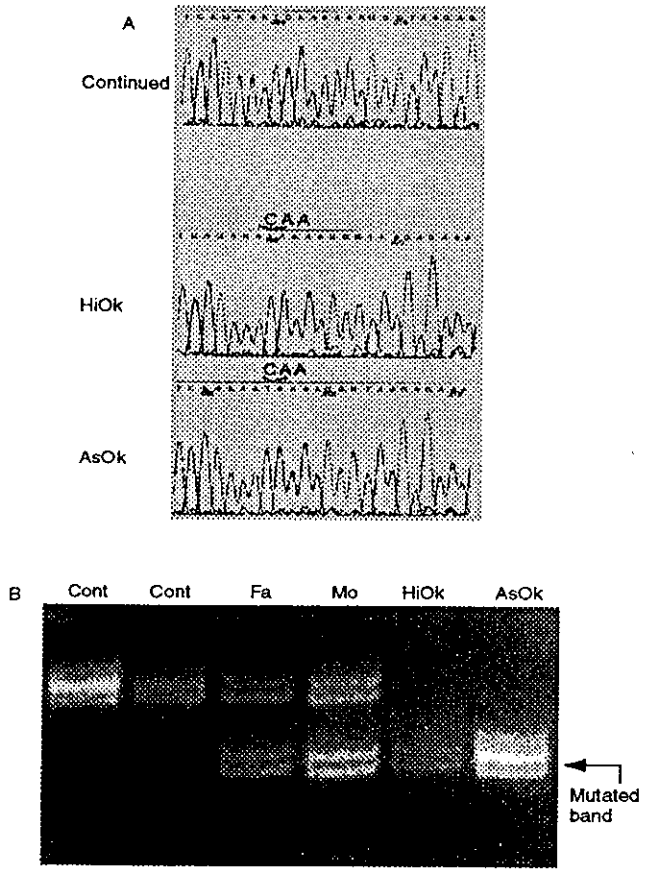

Figure 2. Mutation of BLM gene. BLM (residues 514-741) was amplified by PCR and electrophoresed in 12% acrylamide gel for 30 h at 400 V.
Lane: 1,2: healthy control; 3: father; 4: mother; 5: HiOk; 6: AsOk.
514-741 reveals the position of nucleotides identified in in the BLM cDNA H1-5' [18].

In the BLM protein, the *C*-terminal region plays a crucial role in the proper function of BLM. In contrast to WRN, reported BLM mutations are assumed to lose their helicase activity. This, in part, is affected by the information based on the small number of BLM mutations in BS patients. Observations have showed that correct BLM function requires both intact helicase activity and an intact NLS in the *C*-terminus. Therefore, the mutation of NLS could cause BS as well as the mutations, which abolish the helicase activity of BLM

Expression of BLM gene in peripheral blood mononuclear cells & fetal tissues

Since the BLM protein is relatively large, identification of the gene mutation in the BLM gene for the diagnosis of BS is laborious. Therefore, for screening BS patients, the expression of the BLM protein and nuclear dot formation were investigated. This was performed in EBV-transformed lymphoblastoid cell lines and phytohemagglutinin (PHA)-induced lymphoblastoid cells originating from control and BS patients [28]. In order to search for the source of BLM protein expression, BLM gene expression was investigated. As already described, BLM was expressed in freshly prepared peripheral blood mononuclear cells (PBMCs) and fetal tissues, although the EBV-transformed B-cell line expressed BLM strongly. PBMCs stimulated with PHA showed slight induction of BLM expression. BLM expression in human fetal tissues was investigated by northern blotting. The fetal kidney, heart and liver scarcely expressed BLM. BLM expression was strongly detected in the 7-week-old brain in contrast to the adult brain. As fetal neurons proliferated, BLM might be expressed. In a whole embryo, BLM is strongly expressed at 6 weeks.

Expression of BLM protein in hematopoietic cell lines & PHA-stimulated PBMCs

BLM expression in various hematopoietic cell lines was investigated using polyclonal BLM antibodies. A 160-kDa protein was detected in control EBV-transformed cell lines. By immunoblotting, the 160-kDa band was strongly detected in hematopoietic leukemic cell lines including B-cells, T-cells and myelomonocytes. Ten more control cell lines were examined and the BLM protein was clearly detected in all of these cell lines when 30 µg of protein was loaded. However, in EBV cell lines obtained from BS patients (3403F and H9152 BS cell lines purchased from the American Type Culture Collection [ATCC]), BLM was not detected. In freshly isolated PBMCs, BLM was scarcely detected. As the amount of BLM protein was very low in quiescent PBMCs, it was predicted that this might also be partly reflected in BLM mRNA levels. However, in PHA-stimulated lymphoblasts, expression of BLM protein was significantly induced. The induction of BLM protein started at day 2 after stimulation and continued until day 5. However, PHA-stimulated lymphoblasts from AsOk showed no induction of BLM protein.

Immunohistochemical analysis of the BLM protein was then performed (FIGURE 4). In the control EBV cell line, nuclear dot formation was observed. When stimulated with PHA, some PBMCs exhibited nuclear dots in the nucleus, while others did not, suggesting that nuclear dot formation depends on the cell cycle of each cell. However, in PHA-stimulated PBMCs obtained from BS, no dot formation was observed. PBMCs from AsOk showed levels of ^{3}H-thymidine incorporation (51337cpm) comparable with PBMCs from healthy control (37700–62400cpm), indicating normal activation of peripheral T-cells in the BS patient.

The combined analysis of immunoblotting and immunohistochemistry is thus a useful approach for laboratory diagnosis of BS.

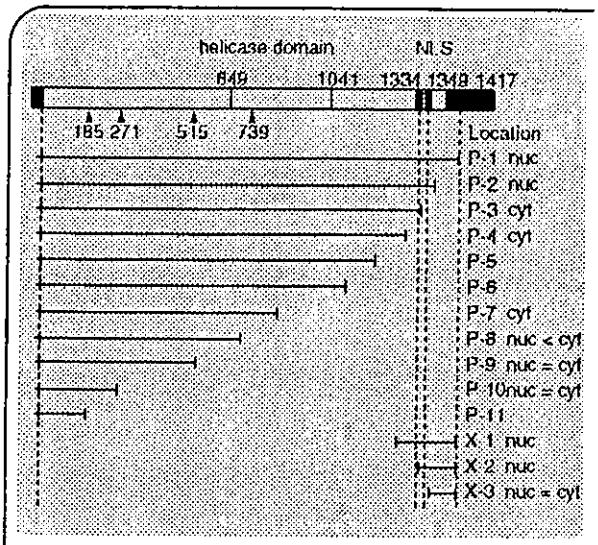

Figure 3. Summary of the localization of GFP-BLM fusion proteins and the DNA fragments of BLM used in these experiments. The numbers show the position of amino acid residues in BLM protein. Arrowheads reveal the position of non-sense mutations in a previously reported manuscript. In those cases where the subcellular location was not exclusively nuclear or cytoplasmic, the results are given by nuc > cyt, nuc = cyt, or nuc < cyt to indicate the predominant pattern of staining observed in transfected cells.
cyt: Cytoplasmic localization of GFP in all cells observed; GFP: Green fluorescent protein; nuc: Nuclear localization of GFP in all cells observed.

Proteins associated with BLM

BLM physically and functionally interacts with an array of proteins whose primary role is the maintenance of genome integrity, such as p53, topoisomerase IIα and SUMO-1 (FIGURE 5) [29–33]. It was found that BLM formed dots/rod-like structures associated with SUMO-1 in the nucleus, for which the region from amino acids 238–586 of BLM is required. The biological relevance of the formation of these dot-like structures, which are associated with SUMO-1, is unclear at present. Meetei and coworkers reported the purification and analysis of proteins in three BLM-associated multiprotein complexes from HeLa cells [34]. Interestingly, one of these complexes includes five Fanconi anemia core complex proteins, which suggests a functional connection between the pathways disturbed in these genomic instability syndromes.

BLM interacts directly with ataxia telangiectasia mutated protein

The BS phenotype suggests that BLM plays a role in recognizing abnormal structures in DNA and suppressing recombinational events that lead to genomic instability. To understand the role of BLM in maintaining genomic stability more fully, the yeast two-hybrid system was initially employed to identify proteins that interact with and influence the function of BLM. Sequence analysis of two strongly positive clones identified a 5.5 kb fragment from the *C*-terminus of the ataxia telangiectasia mutated protein (ATM) cDNA and BLM cDNA. Self-interaction is in keeping with other results, which demonstrate that BLM forms hexameric ring structures [35].

BLM bound to glutathione S-transferase (GST)-ATM-1 (amino acid residues 1–257), GST-ATM-10 (residues 2427–2641) and GST-ATM-12 (residues 2682–3012) in reactions without ethidium bromide. However, when this was included, GST-ATM-1 and GST-ATM-12 were found to bind equally well to BLM but there was reduced interaction with GST-ATM-10. Binding of BLM to GST-ATM-10, which contains the kinase domain of ATM, is consistent with this protein being a substrate for ATM kinase. Binding studies with 35S-labeled BLM revealed that the smallest region of overlap was a sequence of roughly 24 nucleotides, which corresponds to amino acids 82–89. Mapping the region of interaction in BLM was carried out using four overlapping GST fusions (GST 1–4, numbered from the *N*-terminus). Binding of GST-BLM-3 (amino acid residues 636–1074) to ^{35}S-labeled full-length ATM was observed. This data suggests that ATM and BLM function together to recognize abnormal DNA structures by direct interaction.

Knockout mice

Several laboratories have reported the establishment of BLM knockout mice [36,37]. The features of the knockout mice showed striking differences, since the disruption was achieved using different strategies.

However, unlike human BS, three of the knockout mice showed embryonic lethality and only one developed to maturity. Chester and coworkers reported that mice which are homozygous for a targeted mutation in murine BLM are developmentally delayed and die by embryonic day 13.5. Cultured murine BLM$^-$ fibroblasts showed high numbers of SCEs. The growth retardation in mutant embryos can be accounted for by a wave of increased apoptosis. The mutant embryos do not survive past day 13.5 and exhibit severe anemia at that time.

Luo and coworkers reported on mice homozygous for a BLM allele with a duplicated exon 3, which do not express detectable BLM protein. The cell lines from these mice show elevations in the rates of mitotic recombination. The

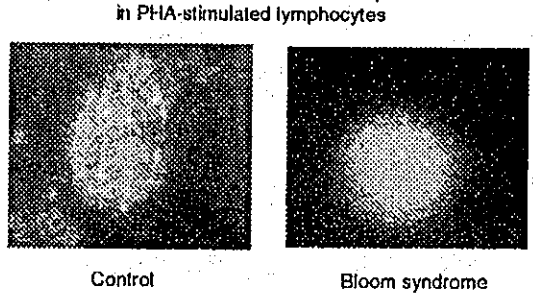

Figure 4. Nuclear dot formation of BLM in phytohemagglutinin-stimulated peripheral blood mononuclear cells from control and Bloom syndrome patient (AsOk).